Nonlinear Dyn
https://doi.org/10.1007/s11071-024-09823-1

RESEARCH

Probabilistic analysis of nonlinear oscillators under correlated multi-power velocity multiplicative excitation and additive excitation

Guo-Peng Bai · Guo-Kang Er · Vai Pan Iu

Received: 26 February 2024 / Accepted: 29 May 2024

Abstract This paper adopts an optimization-oriented exponential-polynomial-closure (OEPC) approach for conducting probabilistic analyses of oscillators under correlated multi-power velocity multiplicative excitation and additive excitation using the idea of exponential polynomial and for extending the conventional EPC method. While the EPC method uses the projection of the residue of the reduced FPK equation to formulate algebraic equations, the OEPC approach minimizes the residue square to handle the stochastic problem. The optimization process entails constructing an objective function (OBJ) with a weight function. The unknown coefficients in the exponential polynomial for estimating the probabilistic solution are then determined by minimizing the OBJ using a gradient-based method. The OEPC approach leads to an approximate probabilistic solution to the system response, which allows for statistical evaluations, such as the mean up-crossing rate. Four examples are provided to demonstrate the effectiveness of the OEPC approach in computing the asymmetric probabilistic solution of the stochastic oscillators with both odd and even nonlinear terms and subjected to correlated multi-power velocity multiplicative excitation and additive excitation. In particular, the verification of the solutions is done by comparison with both Gaussian closure method and Monte Carlo simulation to test the accuracy and reliability of the OEPC approach.

Keywords Nonlinear stochastic oscillator · Probabilistic density function · FPK equation · Exponential-polynomial closure · Optimization

G.-P. Bai (✉) · G.-K. Er · V. P. Iu
Department of Civil and Environmental Engineering, University of Macau, Avenida da Universidade, Taipa 999078, Macau Special Administrative Region, People's Republic of China
e-mail: yc07450@um.edu.mo

G.-K. Er
e-mail: gker@um.edu.mo

V. P. Iu
e-mail: vaipaniu@um.edu.mo

1 Introduction

The probabilistic solutions of random systems have numerous applications in the field of engineering, including the study of structural reliability and risk analysis. Unpredictable failure can appear under random loading conditions, which may result in a significant impact on the safety and reliability of the structures like dams, bridges and towers [1,2]. Random and unpredictable natural phenomena, such as wind, can pose a hazard to buildings and other structures. There were some well-known events that were caused by wind flow, i.e. Tacoma Bridge event (1940) [3], Lodemann Bridge event (1972) [4] and Humen Bridge event (2020) [5]. For the wind-excited or self-excited tower, dynamic analysis has been applied to explore the impact of turbulence on towers, as evidenced in several studies [6–9]. However, relatively few studies have been conducted on the probabilistic

Published online: 15 June 2024

analysis of the system considering the randomness of wind turbulence. In this article, a probabilistic analysis is conducted on an established system through optimization-oriented exponential-polynomial-closure (OEPC) approach. This approach is based on the exponential polynomial assumption of the traditional EPC method [10,11] and extends it through an optimization solution procedure.

There are numerous methods to acquire the probabilistic solution, namely the probability density function (PDF), for the responses of random systems. Although exact solutions are rare to handle practical issues or problems, such solutions remain the first choice whenever available [12,13]. Numerical methods such as Monte Carlo Simulation (MCS) are commonly employed for obtaining the numerical solutions. However, the application of MCS is always constrained by the inefficiency and time consuming [14–18].

The semi-analytical methods are frequently employed in handling real-world problems. Moment functions of first two orders can be obtained using equivalent linearization [19–21]. The Gaussian closure method (GCM) can be applied to solve weakly nonlinear problems using lower-order moments [22,23]. Building upon the equivalent linearization method, the statistical linearization method combines the harmonic balance method to solve the system under both periodic and random excitation [24]. Utilizing the path integration (PI) technique, it is feasible to obtain the PDF of a given system without solving Fokker-Planck-Kolmogorov (FPK) equation [25–28]. The cell mapping method divides the state space into a limited quantity of cells, being computationally efficient than the path integration method in some cases [29–31]. An extrapolation approach is recently developed to improve the computational efficiency of PI, exhibiting high solution accuracy between the current and the extrapolated points [32]. The computational efficiency of PI can also be improved by utilizing sparse PDF expansion, which can be determined by $L_{1/2}$-norm minimization formulation [33]. The stochastic averaging method is applicable for the weakly damped and excited system [34–36]. Basing on a high-order finite difference procedure and utilizing the inverse Fourier transformation, the PDF solution can be estimated [37]. The random vibration behavior of a nonlinear oscillator can be examined through the application of the nonlinear energy sink method [38,39]. By developing the pole-residue transfer function, the pole-residue method is able to provide nonstationary response statistics for the systems subjected to modulated white noise excitation [40]. The exponential-polynomial-closure (EPC) method can solve strongly nonlinear problems, particularly for estimating the tails of PDF solution, as well as the system under Gaussian or Poisson white noise, parametric excitation and with various nonlinear terms [10,41–43]. As for high-dimensional problems, it is suggested to combine the state-space-split method for applications, such as in the analysis of geometrically nonlinear plates [44], stretched Bernoulli beams [45], and the random characteristics analysis of cables [46]. By the results from detailed balance method, the EPC method is further extended [47,48]. Recently, the EPC method has been expanded to acquire the transient or non-stationary PDF solutions of nonlinear stochastic oscillators [11,49–52].

This paper presents the OEPC approach for random vibration analysis, which introduces an alternative way for determining the values of variables in the traditional EPC expression. Utilizing the expression of exponential polynomial, the objective function (hereafter referred to as OBJ) is devised to be the squared residual error of the FPK equation. The unknown coefficients of OEPC are then determined by minimizing the OBJ via a gradient-based method. With this approach, this paper provides an approximate PDF solution for the system response, enabling statistical evaluations such as the mean up-crossing rate (MCR) analysis. To assess the precision of the outcome and the feasibility of the method, four examples based on the established governing equation are given in this paper. The first example is about a system with independent excitations, the second one is about a system with half-correlated excitations, and the third one is about a system with fully correlated excitations. The last example aims to evaluate the accuracy of the solution for higher values of coefficients in the nonlinear damping part. The effectiveness of the presented approach in solving nonlinear oscillations under correlated additive excitation and multiplicative excitation (on powered velocity) has been verified based on the results obtained from the examples.

2 Formulation of FPK equation

The stochastic oscillator being analyzed can be mathematically expressed using Eq. (1).

$$\ddot{\Psi} + 2\xi\omega_0\dot{\Psi} + \omega_0^2\Psi + c_1\dot{\Psi}^2 + c_2\dot{\Psi}^3 + c_3 = \gamma_1\dot{\Psi}^3\Omega_1(t) + \gamma_2\dot{\Psi}\Omega_2(t) + \gamma_3\Omega_3(t) \quad (1)$$

where Ψ and $\dot{\Psi}$ are the displacement and velocity, respectively, and $[\Psi, \dot{\Psi}] \in \mathbb{R}^2$; ξ and ω_0 are the damping ratio and natural frequency, respectively; c_1 and c_2 are the coefficients of $\dot{\Psi}^2$ and $\dot{\Psi}^3$, respectively. It is noted that the term $c_1\dot{\Psi}^2$ can cause even nonlinearity and $c_3\dot{\Psi}^3$ can cause odd nonlinearity in the oscillator. c_3 denotes a constant. The system is subjected to three unit Gaussian white noise excitations denoted as $\Omega_i(t)$ $(i = 1, 2, 3)$ with power spectral density (PSD) $\frac{1}{2\pi}$. $\Omega_1(t)$ corresponds to the multiplicative excitation of the cubic velocity term $(\dot{\Psi}^3)$, and $\Omega_2(t)$ corresponds to the multiplicative excitation of the primary velocity term $(\dot{\Psi})$. These two denote the multi-power velocity multiplicative excitation. $\Omega_3(t)$ corresponds to the additive excitation. The coefficients of each excitation, γ_i $(i = 1, 2, 3)$, reflect the intensities of their respective parts.

Without loss of generality, the excitation described in Eq. (1) is capable of representing the Gaussian white noise with a power spectral density that is not equal to $\frac{1}{2\pi}$. For instance, one can set $\Omega_3^e(t) = \gamma_3\Omega_3(t)$, where the power spectral density of $\Omega_3^e(t)$ will be $\frac{\gamma_3^2}{2\pi}$.

The current scope of this study is limited to solving problems under Gaussian excitations. However, since Poisson white noise (a typical non-Gaussian excitation) is also governed by the FPK equation [43], the OEPC method is still feasible. Therefore, the procedure for solving the problem under Gaussian excitation can be extended to solve the problem under non-Gaussian excitation using different types of FPK equations.

Setting $\Psi = \Psi_1$, $\dot{\Psi} = \Psi_2$ and $h(\Psi_1, \Psi_2) = 2\xi\omega_0\Psi_2 + \omega_0^2\Psi_1 + c_1\Psi_2^2 + c_2\Psi_2^3 + c_3$, the Stratonovich form of Eq. (1) can be written as

$$\begin{cases} \dot{\Psi}_1 = \Psi_2 \\ \dot{\Psi}_2 = -h + \gamma_1\Psi_2^3\Omega_1(t) + \gamma_2\Psi_2\Omega_2(t) + \gamma_3\Omega_3(t) \end{cases} \quad (2)$$

$\Omega_{1,2,3}(t)$ are characterized by

$$\begin{cases} E[\Omega_i(t)]=0, & i = 1, 2, 3; \\ E[\Omega_i(t)\Omega_i(t+\tau)]=\delta(\tau), & i=1, 2, 3; \\ E[\Omega_i(t)\Omega_j(t+\tau)]=\rho_{ij}\delta(\tau), & i\neq j,\ i,\ j=1, 2, 3; \end{cases} \quad (3)$$

where τ denotes the time lag; δ denotes the Dirac function; ρ_{ij} is the correlation coefficient between $\Omega_i(t)$ and $\Omega_j(t)$.

The formulation of the following reduced FPK equation for the stationary PDF solution $p(\psi_1, \psi_2)$ is a consequence of the Markovian property of the two random processes Ψ_1 and Ψ_2 in Eq. (2).

$$\frac{\partial(\psi_2 p)}{\partial\psi_1} - \frac{\partial(hp)}{\partial\psi_2} + \frac{1}{2}\frac{\partial(\beta_1 p)}{\partial\psi_2} - \frac{1}{2}\frac{\partial^2(\beta_2 p)}{\partial\psi_2^2} = 0 \quad (4)$$

where

$$\begin{aligned} \beta_1 &= 3\gamma_1^2\psi_2^5 + 4\rho_{12}\gamma_1\gamma_2\psi_2^3 + 3\rho_{13}\gamma_1\gamma_3\psi_2^2 \\ &\quad + \gamma_2^2\psi_2 + \rho_{23}\gamma_2\gamma_3; \\ \beta_2 &= \gamma_1^2\psi_2^6 + 2\rho_{12}\gamma_1\gamma_2\psi_2^4 + 2\rho_{13}\gamma_1\gamma_3\psi_2^3 \\ &\quad + \gamma_2^2\psi_2^2 + 2\rho_{23}\gamma_2\gamma_3\psi_2 + \gamma_3^2. \end{aligned} \quad (5)$$

In addition, it is assumed that $p(\psi_1, \psi_2)$ fulfills the following conditions.

$$\begin{cases} p(\psi_1, \psi_2) > 0, [\psi_1, \psi_2] \in \mathbb{R}^2 \\ \lim_{\psi_i\to\infty} p(\psi_1, \psi_2) = 0, i = 1, 2 \\ \int_{-\infty}^{+\infty}\int_{-\infty}^{+\infty} p(\psi_1, \psi_2)d\psi_1 d\psi_2 = 1 \end{cases} \quad (6)$$

3 Procedure of OEPC approach

3.1 Formulation of residual error

In accordance with the conventional EPC methods, the PDF solution to Eq. (4) is given as follows [10].

$$\tilde{p}_n(\boldsymbol{\psi}; \boldsymbol{\alpha}) = C\exp(Q_n(\boldsymbol{\psi}; \boldsymbol{\alpha})) \quad (7)$$

where $\boldsymbol{\psi}$ denotes $[\psi_1, \psi_2]$; $\boldsymbol{\alpha}$ is the coefficient vector to be determined; $\tilde{p}_n$ is the approximate PDF with the same order as Q_n; C is a normalization constant; the polynomial, Q_n, is expressed as

$$Q_n(\boldsymbol{\psi}; \boldsymbol{\alpha}) = \alpha_1\psi_1 + \alpha_2\psi_2 + ... + \alpha_N\psi_2^n \quad (8)$$

where the highest order of ψ_i in Q_n is denoted by n; the number of components in Q_n is $N = \frac{n}{2}(n + 3)$; $[\alpha_1, \alpha_2, ..., \alpha_N]^T$ forms the coefficient vector $\boldsymbol{\alpha}$; further details regarding the terms in Q_n are exhibited in Table 1.

Table 1 Polynomial terms in Q_n

$n=6$	$n=4$	$n=2$	$\alpha_1\psi_1$	$\alpha_2\psi_2$				
			$\alpha_3\psi_1^2$	$\alpha_4\psi_1\psi_2$	$\alpha_5\psi_2^2$			
			$\alpha_6\psi_1^3$	$\alpha_7\psi_1^2\psi_2$	$\alpha_8\psi_1\psi_2^2$	$\alpha_9\psi_2^3$		
			$\alpha_{10}\psi_1^4$	$\alpha_{11}\psi_1^3\psi_2$	$\alpha_{12}\psi_1^2\psi_2^2$	$\alpha_{13}\psi_1\psi_2^3$	$\alpha_{14}\psi_2^4$	
			$\alpha_{15}\psi_1^5$	$\alpha_{16}\psi_1^4\psi_2$	$\alpha_{17}\psi_1^3\psi_2^2$	$\alpha_{18}\psi_1^2\psi_2^3$	$\alpha_{19}\psi_1\psi_2^4$	$\alpha_{20}\psi_2^5$
			$\alpha_{21}\psi_1^6$	$\alpha_{22}\psi_1^5\psi_2$	$\alpha_{23}\psi_1^4\psi_2^2$	$\alpha_{24}\psi_1^3\psi_2^3$	$\alpha_{25}\psi_1^2\psi_2^4$	$\alpha_{26}\psi_1\psi_2^5$ $\alpha_{27}\psi_2^6$
…	…							

The left-hand side of Eq. (4) can be used to obtain the residual error Δ_n by substituting Eq. (7) into it.

$$\Delta_n(\boldsymbol{\psi};\boldsymbol{\alpha}) = C\Bigg[\psi_2\frac{\partial \exp Q_n}{\partial\psi_1} + \left(\frac{1}{2}\frac{\partial\beta_1}{\partial\psi_2} - \frac{1}{2}\frac{\partial^2\beta_2}{\partial\psi_2^2} - \frac{\partial h}{\partial\psi_2}\right)\exp Q_n + \left(\frac{\beta_1}{2} - \frac{\partial\beta_2}{\partial\psi_2} - h\right)\frac{\partial \exp Q_n}{\partial\psi_2} - \frac{\beta_2}{2}\frac{\partial^2 \exp Q_n}{\partial\psi_2^2}\Bigg] \tag{9}$$

The expression presented in Eq. (9) can be further simplified as

$$\Delta_n(\boldsymbol{\psi};\boldsymbol{\alpha}) = \tilde{p}_n(\boldsymbol{\psi};\boldsymbol{\alpha})r_n(\boldsymbol{\psi};\boldsymbol{\alpha}) \tag{10}$$

where

$$r_n(\boldsymbol{\psi};\boldsymbol{\alpha}) = \psi_2\frac{\partial Q_n}{\partial\psi_1} + \frac{1}{2}\frac{\partial\beta_1}{\partial\psi_2} - \frac{1}{2}\frac{\partial^2\beta_2}{\partial\psi_2^2} - \frac{\partial h}{\partial\psi_2} + \left(\frac{\beta_1}{2} - \frac{\partial\beta_2}{\partial\psi_2} - h\right)\frac{\partial Q_n}{\partial\psi_2} - \frac{\beta_2}{2}\left(\frac{\partial^2 Q_n}{\partial\psi_2^2} + \frac{\partial Q_n}{\partial\psi_2}\frac{\partial Q_n}{\partial\psi_2}\right) \tag{11}$$

3.2 Construction of OBJ

In Eq. (10), it is observed that $\Delta_n(\boldsymbol{\psi};\boldsymbol{\alpha})$ consists of two components, namely $\tilde{p}_n(\boldsymbol{\psi};\boldsymbol{\alpha})$ and $r_n(\boldsymbol{\psi};\boldsymbol{\alpha})$. The first component, $\tilde{p}_n(\boldsymbol{\psi};\boldsymbol{\alpha})$, is obtained from Eq. (7), and solely contains exponential terms, ensuring it positive. Hence, to minimize $\Delta(\boldsymbol{\psi};\boldsymbol{\alpha})$ towards zero, the second component, $r_n(\boldsymbol{\psi};\boldsymbol{\alpha})$, must approach zero. Therefore, the expression of $r_n(\boldsymbol{\psi};\boldsymbol{\alpha})$, Eq. (11) is adopted to formulate the OBJ for determining the values of $\boldsymbol{\alpha}$.

$$\Theta_n(\boldsymbol{\alpha}) = \int_{-\infty}^{+\infty}\int_{-\infty}^{+\infty} r_n^2(\boldsymbol{\psi};\boldsymbol{\alpha})\hat{p}_2(\boldsymbol{\psi})d\psi_1 d\psi_2 \tag{12}$$

where Θ_n is the formulated OBJ; $\hat{p}_2(\boldsymbol{\psi})$ is the weighting function which is from GCM, allowing the weighted error to be integrated in closed form.

The weighting function $\hat{p}_2(\boldsymbol{\psi})$ is designed to calculate the integral of the constructed OBJ within $(-\infty, +\infty)$ by replacing the integral terms with the corresponding expectation values. Therefore, the weighting function ensures the integral to be calculated analytically. Comparing to the numerical integration in a finite rage, i.e., $[m-4\sigma, m+4\sigma]$, the analytical integration can improve the accuracy of the result. Therefore, the weighting function enhances the accuracy of the integral calculations.

By employing a gradient-based method, the values of $\boldsymbol{\alpha}$ can be determined through Eq. (13).

$$\min_{\boldsymbol{\alpha}} \Theta_n(\boldsymbol{\alpha}) \tag{13}$$

In the optimization procedure, finding the minimum value of OBJ requires an initial guess, denoted as $\boldsymbol{\alpha}^{(0)}$, to determine the values of the unknown variables. According to empirical evidence, using a Gaussian initial guess helps to achieve a converged solution. A good initial estimate assists in yielding a quality solution and reducing computational time. The detailed procedures for determining $\hat{p}_2(\boldsymbol{\psi})$ and $\boldsymbol{\alpha}^{(0)}$ are presented.

3.3 Weighting function and initial coefficient

When building the OBJ, introducing the weighting function into the spatial integration Eq. (12) helps to

improve the integral accuracy and simplify the calculation. $\hat{p}_2(\boldsymbol{\psi})$ is Gaussian type PDF, which can be expressed as

$$\hat{p}_2(\boldsymbol{\psi};\boldsymbol{\eta}) = C_2 \exp(\eta_1\psi_1 + \eta_2\psi_2 + \eta_3\psi_1^2 + \eta_4\psi_1\psi_2 + \eta_5\psi_2^2) \tag{14}$$

where C_2 serves as a constant for achieving normalization in the equation; $\boldsymbol{\eta}$ is a coefficient vector that can be estimated by GCM as follows.

Linearizing the system from Eq. (2) gives the linearization coefficient equations, which are expressed by

$$\begin{cases} \nu_1 = \dfrac{E[h(\Psi_1,\Psi_2)\Psi_2] - E[h(\Psi_1,\Psi_2)]E[\Psi_2]}{E[\Psi_2^2] - E[\Psi_2]^2} \\ \nu_2 = \dfrac{E[h(\Psi_1,\Psi_2)\Psi_1] - E[h(\Psi_1,\Psi_2)]E[\Psi_1]}{E[\Psi_1^2] - E[\Psi_1]^2} \\ \nu_3 = E[h(\Psi_1,\Psi_2)] - \nu_1 E[\Psi_2] - \nu_2 E[\Psi_1] \end{cases} \tag{15}$$

where ν_1, ν_2, and ν_3 are parameters in the linearized system Eq. (16).

$$\begin{cases} \dot{\Psi}_1 = \Psi_2 \\ \dot{\Psi}_2 = -\nu_1\Psi_2 - \nu_2\Psi_1 - \nu_3 + \gamma_1\Psi_2^3\Omega_1(t) \\ \quad +\gamma_2\Psi_2\Omega_2(t) + \gamma_3\Omega_3(t) \end{cases} \tag{16}$$

The moment equations corresponding to Eq. (16) are listed in Eq. (17).

$$\begin{cases} \nu_1 E[\Psi_2] + \nu_2 E[\Psi_1] + \nu_3 - \dfrac{1}{2}\Big(3\gamma_1^2 E[{\Psi_2}^5] \\ +4\rho_{12}\gamma_1\gamma_2 + E[{\Psi_2}^3] + 3\rho_{13}\gamma_1\gamma_3 E[{\Psi_2}^2] \\ +\gamma_2 E[\Psi_2] + \rho_{23}\gamma_2\gamma_3\Big) = 0 \\ E[\Psi_2] = 0 - E[{\Psi_2}^2] + \nu_1 E[\Psi_1\Psi_2] + \nu_2 E[\Psi_1^2] \\ +\nu_3 E[\Psi_1] - \dfrac{1}{2}\Big(3\gamma_1^2 + E[\Psi_1{\Psi_2}^5] \\ +4\rho_{12}\gamma_1\gamma_2 E[\Psi_1{\Psi_2}^3] + 3\rho_{13}\gamma_1\gamma_3 E[\Psi_1{\Psi_2}^2] \\ +\gamma_2^2 E[\Psi_1\Psi_2] + \rho_{23}\gamma_2\gamma_3 E[\Psi_1]\Big) = 0 \\ -2E[\Psi_1\Psi_2] = 02(\nu_1 E[{\Psi_2}^2] + \nu_2 E[\Psi_1\Psi_2] \\ +\nu_3 E[\Psi_2]) - \Big(4\gamma_1^2 E[{\Psi_2}^6] + 6\rho_{12}\gamma_1\gamma_2 E[{\Psi_2}^4] \\ +5\rho_{13}\gamma_1\gamma_3 E[{\Psi_2}^3] + 2\gamma_2^2 E[{\Psi_2}^2] \\ +3\rho_{23}\gamma_2\gamma_3 E[\Psi_2] + \gamma_3^2\Big) = 0 \end{cases} \tag{17}$$

Equations (15 and 17) contains multiple unknown moments such as $E[\Psi_1^i]$ and $E[\Psi_2^i](i = 1, 2, 3, etc)$. Through simplifying with Eq. (18), only the first two order moments are retained.

$$\begin{cases} E[\Psi_1^i\Psi_2^j] = E[\Psi_1^i]E[\Psi_2^j],\ i, j = 0, 1, 2, \ldots \\ E[\Psi_i^j] = E[\Psi_i]E[\Psi_i^{j-1}] + (j-1)\big(E[\Psi_i^2] \\ -E[\Psi_i]^2\big)E[\Psi_i^{j-2}],\ i = 1, 2;\ j >= 3. \end{cases} \tag{18}$$

After simplification, Eqs. (15 and 17) can be solved by iterative procedure, leading to the values of ν_1, ν_2, ν_3, $E[\Psi_1]$, $E[\Psi_2]$, $E[\Psi_1^2]$ and $E[{\Psi_2}^2]$. Then the unknowns in Eq. (14) can be given by:

$$\begin{cases} \eta_1 = \dfrac{E[\Psi_1]}{E[\Psi_1^2] - E[\Psi_1]^2} \\ \eta_2 = \dfrac{E[\Psi_2]}{E[\Psi_2^2] - E[\Psi_2]^2} \\ \eta_3 = -\dfrac{1}{2(E[\Psi_1^2] - E[\Psi_1]^2)} \\ \eta_4 = 0 \\ \eta_5 = -\dfrac{1}{2(E[\Psi_2^2] - E[\Psi_2]^2)} \\ C_2 = \dfrac{\sqrt{\eta_3\eta_5}}{\pi}\exp\left(-\dfrac{\eta_1}{2}E[\Psi_1] - \dfrac{\eta_2}{2}E[\Psi_2]\right) \end{cases} \tag{19}$$

Using the weight function, the integral $\int_{-\infty}^{+\infty}\int_{-\infty}^{+\infty} * \hat{p}_2 d\psi_1 d\psi_2$ in Eq. (12) can be directly replaced by the value of $E[*]$, where $*$ denotes the polynomial term in the expansion of r_n^2. Additionally, Eq. (18) enables the derivation of higher-order moments, which correspond to higher order terms in r_n^2. Therefore, by utilizing $\hat{p}_2$, Eq. (12) can be analytically integrated within $(-\infty, +\infty)$.

Based on Eq. (19), the initial coefficient required to start the optimization procedure can be obtained. Setting $\alpha_i^{(0)} = 0$ for $i \geq 6$, the initial coefficient vector can be expressed as $\boldsymbol{\alpha}^{(0)} = [\eta_1, \eta_2, \eta_3, \eta_4, \eta_5, 0, 0, \ldots, 0]$.

3.4 Optimization solution procedure

To solve Eq. (13), the Broyden-Fletcher-Goldfarb-Shanno (BFGS) method is adopted [53–56]. The BFGS method is a type of quasi-Newton method, which is also a gradient-based method [57,58]. The fundamental theory of BFGS can be represented by the following equation [59].

$$\boldsymbol{\alpha}^{(j+1)} = \boldsymbol{\alpha}^{(j)} - k_j \boldsymbol{G_j} \nabla\Theta_n(\boldsymbol{\alpha}^{(j)}) \tag{20}$$

where j denotes the number of iteration; k_j is a coefficient to be determined in the procedure of BFGS; G_j is the estimated inverse Hessian matrix; $\nabla\Theta_n(\boldsymbol{\alpha}^{(j)})$ denotes the gradient of Θ_n.

Table 2 BFGS algorithm program procedure

Start...
Initialize vector $\boldsymbol{\alpha}^{(0)}$
Initial approximate inverse Hessian guess $\boldsymbol{G}_0 = I_N$
for $j = 0, 1, 2, ...$
  compute gradient $\boldsymbol{g}^{(j)} = \nabla\Theta_n(\boldsymbol{\alpha}^{(j)})$
  compute search direction $\boldsymbol{d}^{(j)} = -\boldsymbol{G}_j\boldsymbol{g}^{(j)}$
  compute step length $k_j = \text{argmin}_{k\geq 0}\left[\Theta_n(\boldsymbol{\alpha}^{(j)} + k\boldsymbol{d}^{(j)})\right]$
  compute $\boldsymbol{\delta}_{\boldsymbol{\alpha}}^{(j)} = k_j\boldsymbol{d}^{(j)}$
  update $\boldsymbol{\alpha}^{(j+1)} = \boldsymbol{\alpha}^{(j)} + \boldsymbol{\delta}_{\boldsymbol{\alpha}}^{(j)}$
  compute next gradient $\boldsymbol{g}^{(j+1)} = \nabla\Theta_n(\boldsymbol{\alpha}^{(j+1)})$ ▶ save for updating in next loop
  if $||\Theta_n(\boldsymbol{\alpha}^{(j+1)}) - \Theta_n(\boldsymbol{\alpha}^{(j)})|| < \varepsilon_0$ **or** $||\boldsymbol{g}^{(j+1)}|| < \varepsilon_0$
    solution is converged, output $\boldsymbol{\alpha}^* = \boldsymbol{\alpha}^{(j+1)}$ and stop
  else
    compute $\boldsymbol{\delta}_{\boldsymbol{g}}^{(j)} = \boldsymbol{g}^{(j+1)} - \boldsymbol{g}^{(j)}$
    compute $\Delta\boldsymbol{G}_j = \left(1 + \frac{(\boldsymbol{\delta}_{\boldsymbol{g}}^{(j)})^T G_k \boldsymbol{\delta}_{\boldsymbol{g}}^{(j)}}{(\boldsymbol{\delta}_{\boldsymbol{g}}^{(j)})^T \boldsymbol{\delta}_{\boldsymbol{\alpha}}^{(j)}}\right)\frac{\boldsymbol{\delta}_{\boldsymbol{\alpha}}^{(j)}(\boldsymbol{\delta}_{\boldsymbol{\alpha}}^{(j)})^T}{(\boldsymbol{\delta}_{\boldsymbol{\alpha}}^{(j)})^T\boldsymbol{\delta}_{\boldsymbol{g}}^{(j)}} - \frac{G_k\boldsymbol{\delta}_{\boldsymbol{g}}^{(j)}(\boldsymbol{\delta}_{\boldsymbol{\alpha}}^{(j)})^T + (G_k\boldsymbol{\delta}_{\boldsymbol{g}}^{(j)}(\boldsymbol{\delta}_{\boldsymbol{\alpha}}^{(j)})^T)^T}{(\boldsymbol{\delta}_{\boldsymbol{g}}^{(j)})^T\boldsymbol{\delta}_{\boldsymbol{\alpha}}^{(j)}}$
    update $\boldsymbol{G}_{j+1} = \boldsymbol{G}_j + \Delta\boldsymbol{G}_j$
  end if
end for

The BFGS involves initializing an approximate inverse Hessian and updating it at each iteration. The quasi-Newton method are so-called because of using an approximation inverse Hessian instead of the true one [60]. Since computing the inverse of Hessian by the original Newton method can be prohibitively expensive, the BFGS method improves the computational efficiency by updating the approximate inverse Hessian matrix without having to compute it directly [61]. The detailed procedure of BFGS algorithm is shown in Table 2.

In Table 2, I_N is an identity matrix; N is the number of variables in $\boldsymbol{\alpha}$; ε_0 is the iteration stopping criteria which is taken as 10^{-8}; $||*||$ refers to Euclidean norm. The function $\text{argmin}_{k\geq 0}\left[\Theta_n(\boldsymbol{\alpha}^{(j)} + k\boldsymbol{d}^{(j)})\right]$ means that, under the condition $k \geq 0$, the value of k makes $\Theta_n(\boldsymbol{\alpha}^{(j)} + k\boldsymbol{d}^{(j)})$ minimized, which can be regarded as a one-dimensional optimization problem. The problem can be solved by Golden section search method [60]. The value of k can also be approximated by $-\frac{(g^{(j)})^T d^{(j)}}{(d^{(j)})^T H d^{(j)}}$ which is adopted in the following analysis [62].

As shown in Table 2, BFGS is able to ensure a positive-definite matrix approximation that gets updated at every iteration, improving the second-order derivative along the search direction. It is noted that the original Newton method cannot guarantee the positive definiteness of Hessian matrix [63,64]. The loss of the positive definiteness can result in the loss of minimum point in the optimization procedure. Therefore, by approximating the inverse Hessian with a positive-definite matrix, the BFGS method enhance the solution procedure by providing an accurate estimate of the Hessian's inverse with significantly less computational cost [62,65].

4 Example of probability analysis

In this paper, the performance of the OEPC approach is evaluated through the analyses of four different oscillators. The first one is excited using three independent noise sources with $\rho_{i,j} = 0$ $(i \neq j)$. The second one is subjected to three correlated noise sources, where $\rho_{i,j} = 0.5$ $(i \neq j)$. The third one is excited by fully correlated noise sources, where $\rho_{i,j} = 1$ for all $i \neq j$. The fourth oscillator extends the second one with increased nonlinearity. The accuracy of OEPC solutions is assessed by performing a comparison with MCS. Additionally, the results are also compared with those from GCM in each example. All calculations are conducted on a computer equipped with 'CPU: Intel® Core™ i9-12900 H Processor (24 M Cache, up to 5.00 GHz); Memory Module: DDR5(4800Mhz, 16.00GB); and SSD DISK: 512 GB'.

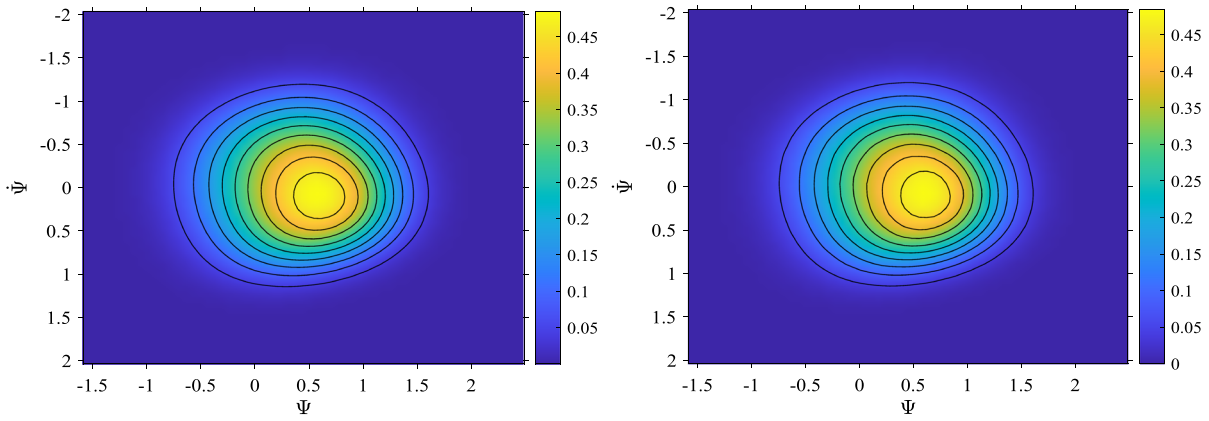

(a) $p(\psi_1, \psi_2)$ of OEPC (b) $p(\psi_1, \psi_2)$ of MCS

Fig. 1 PDF solutions in the case of three independent excitations (Example 1); GCM: $m_1 = 0.4498, m_2 = 0, \sigma_1 = 0.5008, \sigma_2 = 0.5008$

4.1 Example 1

The values of system parameters in Eq. (1) are specified by $\xi = 0.1$, $\omega_0 = 1$, $c_1 = 0.2$, $c_2 = 0.4$, $c_3 = -0.5$, $\gamma_1 = 0.05$, $\gamma_2 = 0.5$, $\gamma_3 = 0.01$. Then the governing equation is given as Eq. (21).

$$\begin{aligned}&\ddot{\Psi} + 0.2\dot{\Psi} + \Psi + 0.2\dot{\Psi}^2 + 0.4\dot{\Psi}^3 - 0.5\\ &= 0.05\dot{\Psi}^3\Omega_1(t) + 0.5\dot{\Psi}\Omega_2(t) + 0.01\Omega_3(t)\end{aligned} \tag{21}$$

The correlation coefficient matrix of the three independent noises is expressed as

$$\rho = \begin{bmatrix} 1 & 0 & 0 \\ 0 & 1 & 0 \\ 0 & 0 & 1 \end{bmatrix} \tag{22}$$

The OBJ for Eq. (1) is specified as

$$\begin{aligned}\Theta_n(\boldsymbol{\alpha}) = \int_{\mathbb{R}^2} \Bigg\{ & \psi_2 \frac{\partial Q_n}{\partial \psi_1} - \frac{15\gamma_1^2}{2}\psi_2^4 \\ & - (3c_2 + 6\rho_{12}\gamma_1\gamma_2)\,\psi_2^2 - (2c_1 + 3\rho_{13}\gamma_1\gamma_3)\,\psi_2 \\ & - 2\xi\omega_0 - \frac{\gamma_2^2}{2} + \frac{\partial Q_n}{\partial \psi_2} \times \Bigg[- \frac{9\gamma_1^2}{2}\psi_2^5 \\ & - (c_2 + 6\rho_{12}\gamma_1\gamma_2)\,\psi_2^3 - \left(c_1 + \frac{9\rho_{13}\gamma_1\gamma_3}{2}\right)\psi_2^2 \\ & - \left(2\xi\omega_0 + \frac{3\gamma_2^2}{2}\right)\psi_2 - \omega_0^2\psi_1 - c_3 - \frac{3\rho_{23}\gamma_2\gamma_3}{2}\Bigg] \\ & - \Bigg(\frac{\gamma_1^2\psi_2^6 + 2\rho_{12}\gamma_1\gamma_2\psi_2^4 + 2\rho_{13}\gamma_1\gamma_3\psi_2^3}{2} \\ & + \frac{\gamma_2^2\psi_2^2 + 2\rho_{23}\gamma_2\gamma_3\psi_2 + \gamma_3^2}{2}\Bigg) \\ & \left(\frac{\partial^2 Q_n}{\partial \psi_2^2} + \frac{\partial Q_n}{\partial \psi_2}\frac{\partial Q_n}{\partial \psi_2}\right)\Bigg\}^2 \hat{p}_2(\boldsymbol{\psi}) d\psi_1 d\psi_2\end{aligned} \tag{23}$$

The minimum of $\Theta_n(\boldsymbol{\alpha})$ is located through the optimization procedure. The obtained PDF solution $p(\psi_1, \psi_2)$ is plotted within $[m - 4\sigma, m + 4\sigma]$ in Fig. 1. m and σ denote the mean and standard deviation from GCM in all examples. m_i and σ_i correspond to the state variable ψ_i $(i = 1, 2)$.

The estimated $p(\psi_1, \psi_2)$ is shown in Fig. 1a. Figure 1b presents the solution of MCS with the sample size 3×10^8. The PDF solution obtained through the OEPC method shows a strong resemblance to the PDF solutions derived from MCS, as can be noted by observation. The PDFs $p(\psi_1)$ and $p(\psi_2)$ can be got by integrating $p(\psi_1, \psi_2)$. The logarithmic marginal PDFs from MCS, GCM and OEPC $(n = 6)$ are plotted in Fig. 2.

In Fig. 2, the curve of GCM represents the solution from GCM, which is also used as the initial guess for the OEPC method. As depicted in Fig. 2, the PDFs of OEPC exhibit excellent agreement with the solutions of MCS, and significantly improve in comparison to the solutions obtained via GCM.

In application, the MCR is used to estimate the reliability of extreme events such as wind loads or fatigue crack growth in structures [66,67]. MCR can also be used in the benchmark studies to evaluate the accuracy and reliability of civil engineering structures [68,69]. It is known that MCR (ν_G^+) from GCM can be directly obtained by Eq. (24) and non-Gaussian MCR (ν^+) need to be integrated by Eq. (25) [70].

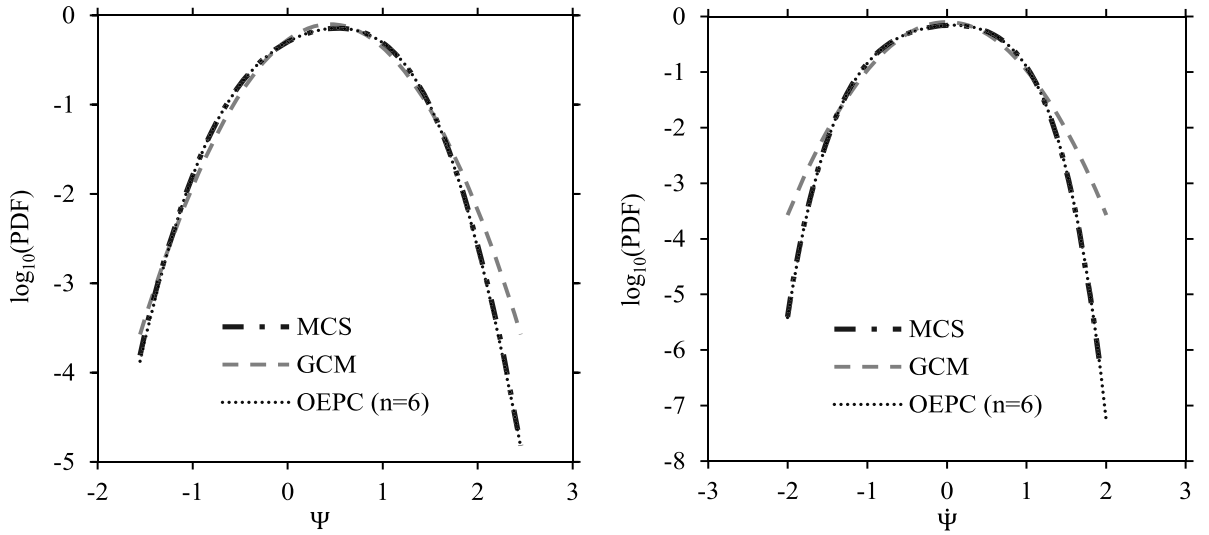

(a) $\log_{10} p(\psi_1)$ of MCS, GCM and OEPC (b) $\log_{10} p(\psi_2)$ of MCS, GCM and OEPC

Fig. 2 Logarithmic PDF solutions of the responses Ψ and $\dot{\Psi}$ and their comparison (Example 1)

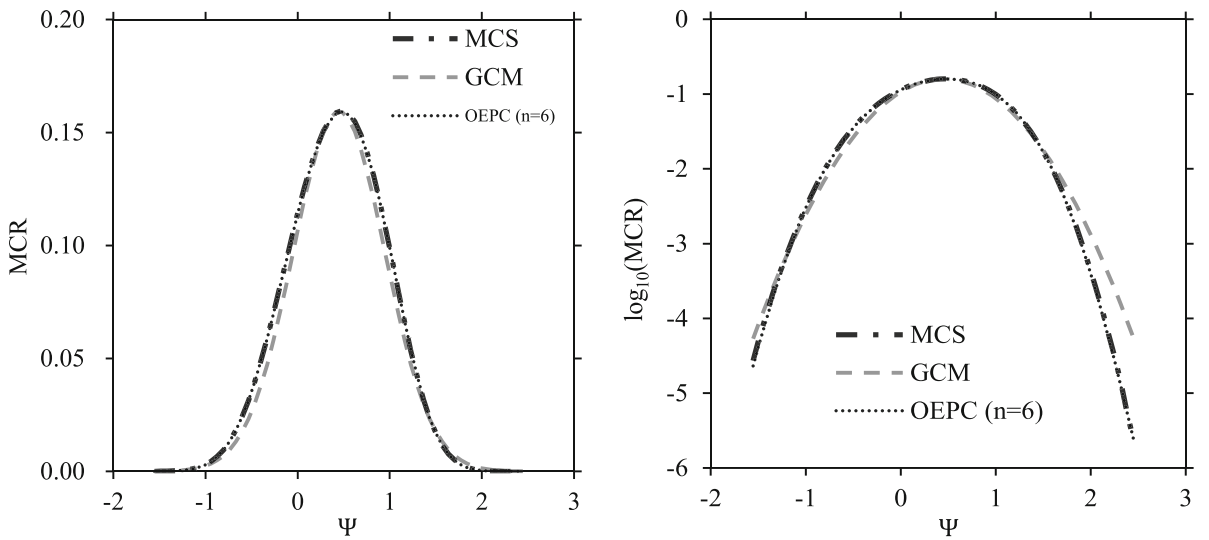

(a) MCR of MCS, GCM and OEPC (b) $\log_{10}$MCR of MCS, GCM and OEPC

Fig. 3 MCR and Logarithmic MCR (Example 1)

$$\nu_G^+(\psi_1) = \frac{\sigma_2}{2\pi\sigma_1} \exp\left[-\frac{(\psi_1 - m_1)^2}{2\sigma_1^2}\right] \tag{24}$$

$$\nu^+(\psi_1) = \int_0^\infty \psi_2 p(\psi_1, \psi_2) d\psi_2 \tag{25}$$

The MCR and $\log_{10}$ MCR are illustrated in Fig. 3. It demonstrates that the MCR obtained by the OEPC approach almost coincides with that of MCS and significantly surpasses the GCM result. These findings indicate the advantage of the OEPC technique. In addition, the total time of OEPC (45 s) is the sum of the time spent by GCM (1.95s) and the time spent on formulation and optimization procedures (42.75s). The time required for computation of MCS (3×10^8) is 3257 s, while the OEPC approach with $n = 6$ only requires 45 s, which highlights the efficiency of the OEPC approach.

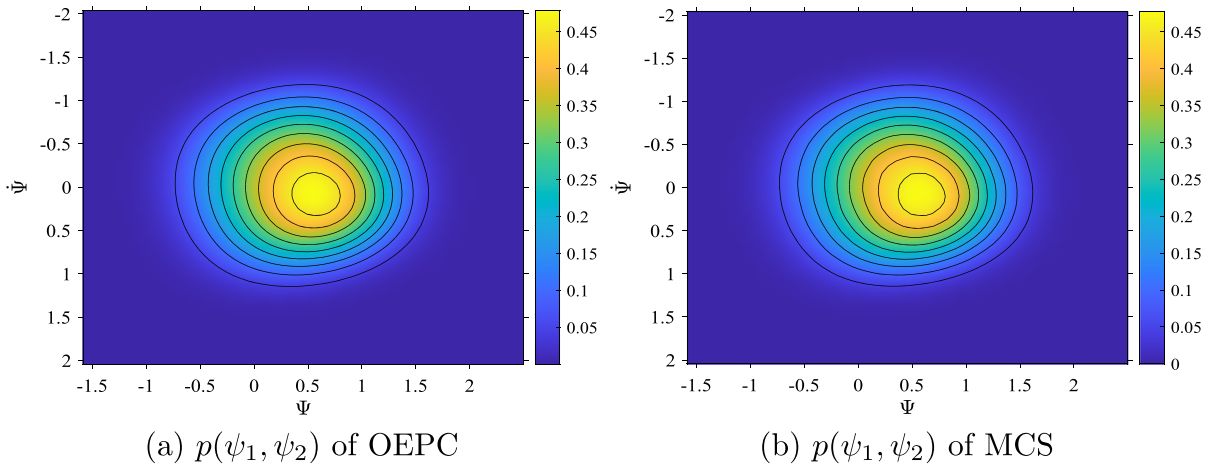

(a) $p(\psi_1, \psi_2)$ of OEPC (b) $p(\psi_1, \psi_2)$ of MCS

Fig. 4 PDF solutions in the case of three half correlated excitations (Example 2); GCM: $m_1 = 0.4559$, $m_2 = 0$, $\sigma_1 = 0.5023$, $\sigma_2 = 0.5022$

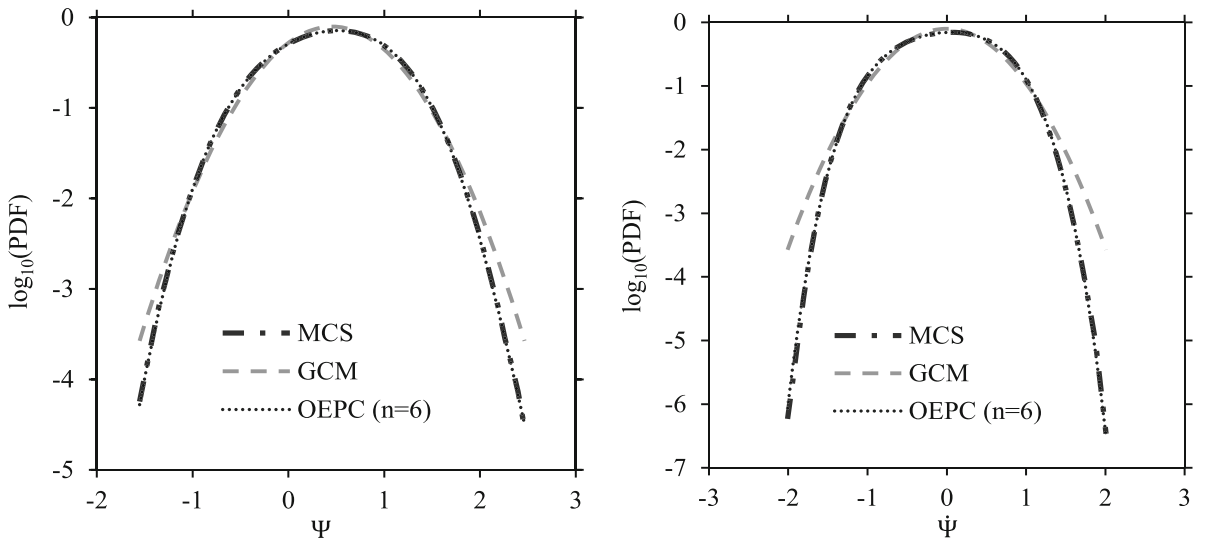

(a) $\log_{10} p(\psi_1)$ of MCS, GCM and OEPC (b) $\log_{10} p(\psi_2)$ of MCS, GCM and OEPC

Fig. 5 Logarithmic PDF solutions of the responses Ψ and $\dot{\Psi}$ and their comparison (Example 2)

4.2 Example 2

Equation (21) can also be used to express the system in Example 2. However, the correlation coefficient matrix for the three noises differs from that in Example 1. The matrix is given as follows:

$$\rho = \begin{bmatrix} 1 & 0.5 & 0.5 \\ 0.5 & 1 & 0.5 \\ 0.5 & 0.5 & 1 \end{bmatrix} \tag{26}$$

The PDF solutions of the OEPC and MCS within $[m - 4\sigma, m + 4\sigma]$ are presented in Fig. 4. Notably, the $p(\psi_1, \psi_2)$ obtained from the OEPC method remains excellent agreement with that determined by the MCS.

In Fig. 5, the logarithmic marginal PDF solutions are plotted with MCS, GCM and OEPC ($n = 6$). The corresponding figures reveal that the PDFs yielded by the OEPC method are almost identical to those of MCS and outperform those by the GCM approach.

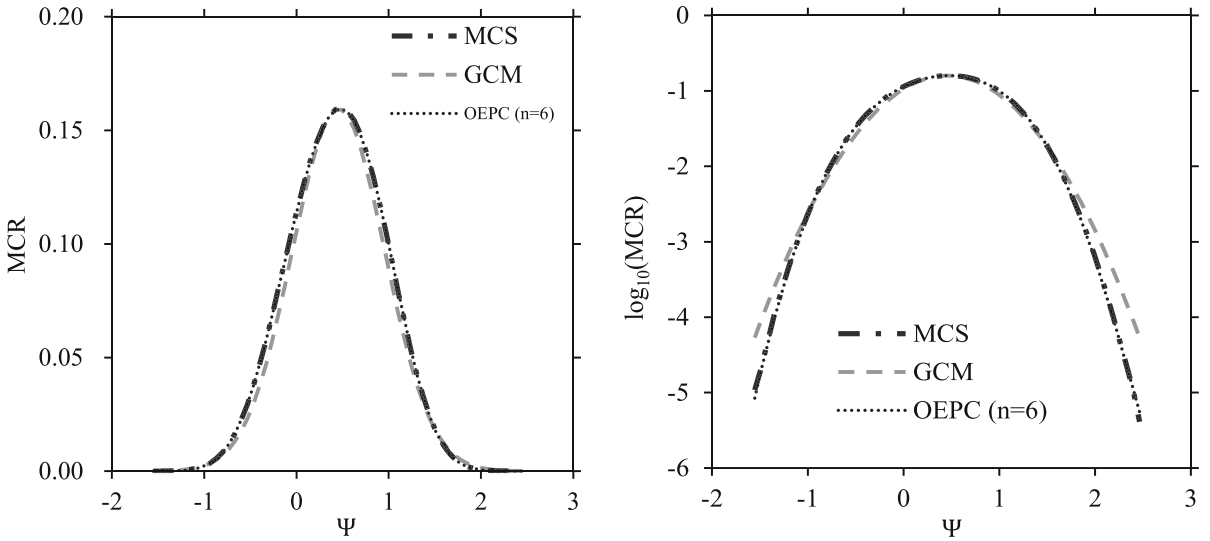

(a) MCR of MCS, GCM and OEPC (b) $\log_{10}$MCR of MCS, GCM and OEPC

Fig. 6 MCR and Logarithmic MCR (Example 2)

The MCR comparisons among OEPC, MCS and GCM are presented in Fig. 6. The OEPC's MCR aligns favorably with MCS's, surpassing GCM's significantly. The total time of OEPC (53 s) is the sum of the time spent by GCM (1.88s) and the time spent on formulation and optimization procedures (50.66s). Remarkably, the OEPC technique completes the calculations in just 53 s, whereas the MCS (3×10^8) requires 3223 s. This indicates that the OEPC method offers a speed advantage of approximately 60 times compared to MCS in this case. These results suggest that the OEPC method has the potential to enhance the efficiency and accuracy for the probabilistic analysis.

4.3 Example 3

The system parameters in Example 3 are the same as those in Eq. (21), except for the correlation coefficient matrix of the noises. The matrix is expressed as follows:

$$\rho = \begin{bmatrix} 1 & 1 & 1 \\ 1 & 1 & 1 \\ 1 & 1 & 1 \end{bmatrix} \tag{27}$$

The matrix Eq. (27) is not positive definite, meaning that the computation of the Cholesky decomposition for ρ is invalid, making the MCS procedure incapable. Thus, it is essential to provide an alternative way to address this issue. Since the PSDs of $\Omega_i(t)$ $(i = 1, 2, 3)$ are the same in this case, it is possible to describe the analyzed oscillator with a single noise term, which is denoted as $\Omega(t) = \Omega_i(t)$. Hence, Eq. (21) can be further expressed as

$$\begin{aligned} &\ddot{\Psi} + 0.2\dot{\Psi} + \Psi + 0.2\dot{\Psi}^2 + 0.4\dot{\Psi}^3 - 0.5 \\ &\quad = 0.05\dot{\Psi}^3\Omega(t) + 0.5\dot{\Psi}\Omega(t) + 0.01\Omega(t) \end{aligned} \tag{28}$$

In real application, such as the towers or bridges that are subjected to wind from different directions, the external and parametric excitations are typically considered from one wind source, resulting in full correlation. Consequently, as demonstrated in several studies [6–9], the system subjected to a single wind source can be used to analyze the impact of wind turbulence on frame towers, which provides a realistic background for Eq. (28).

The PDF solutions to Eq. (28) are presented in Fig. 7. In this case, the bivariate PDF of OEPC (with $n = 6$) exhibits a remarkable similarity to the solution from MCS within $[m - 4\sigma, m + 4\sigma]$.

Furthermore, in Fig. 8, the logarithmic marginal PDF solutions of OEPC are almost identical to those of MCS and superior to those of GCM.

The MCRs from MCS, GCM and OEPC ($n = 6$), are presented in Fig. 9, where it can be observed that the MCR from OEPC is consistent with MCS and surpasses that of GCM. Furthermore, the total time of OEPC

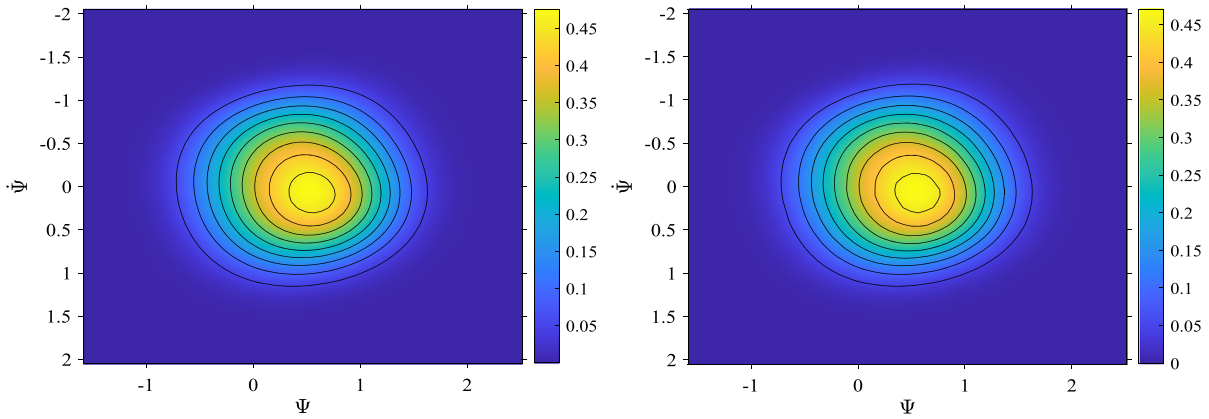

(a) $p(\psi_1, \psi_2)$ of OEPC (b) $p(\psi_1, \psi_2)$ of MCS

Fig. 7 PDF solutions in the case of three fully correlated excitations (Example 3); GCM: $m_1 = 0.4619$, $m_2 = 0$, $\sigma_1 = 0.5037$, $\sigma_2 = 0.5036$

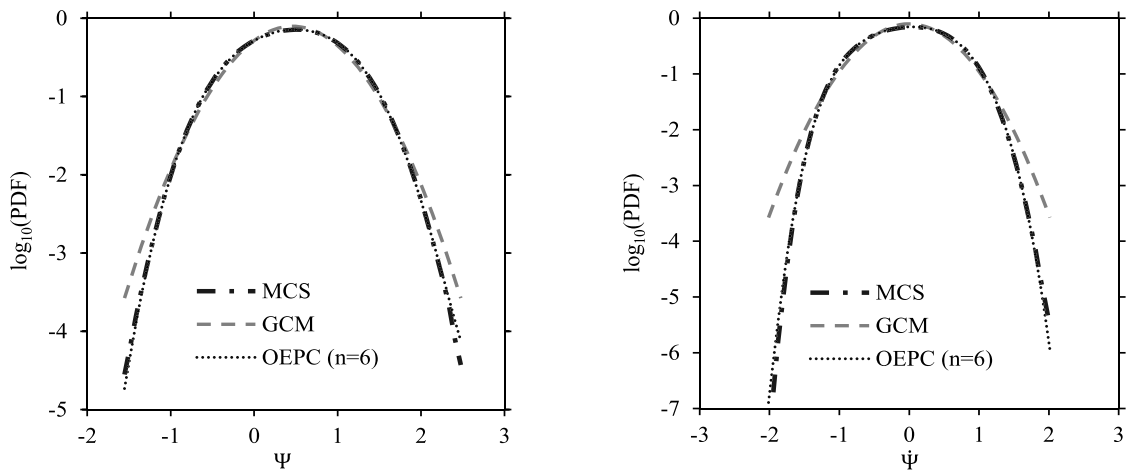

(a) $\log_{10} p(\psi_1)$ of MCS, GCM and OEPC (b) $\log_{10} p(\psi_2)$ of MCS, GCM and OEPC

Fig. 8 Logarithmic PDF solutions of the responses Ψ and $\dot{\Psi}$ and their comparison (Example 3)

(53 s) is the sum of the time spent by GCM (1.20s) and the time spent on formulation and optimization procedures (51.72s). The computational time of MCS is 2929 s, while OEPC only takes 53 s, resulting in a significant time reduction.

4.4 Impact of correlation coefficients

Examples 1, 2 and 3 correspond to the systems under independent excitations, half-correlated excitations, and fully correlated excitations, respectively. Comparing the logarithmic PDF solutions of the three examples in Fig. 10, it can be observed that the length of their left and right arms is different. This indicates that the correlation coefficients have an influence on the tail behavior of the PDF solution, which is similar to the phenomenon described in [71].

The difference in logarithmic PDFs is attributed to the variation in the PDF solutions from Figs. 1, 4 and 7. Since the contour lines in the bottom right quadrant of Fig. 1 are slightly denser than those in Figs. 4 and 7, it indicate a steeper joint PDF and faster changes of the values in that region. In addition, the peak in Fig. 7 moves slightly to the upper left compared to those in

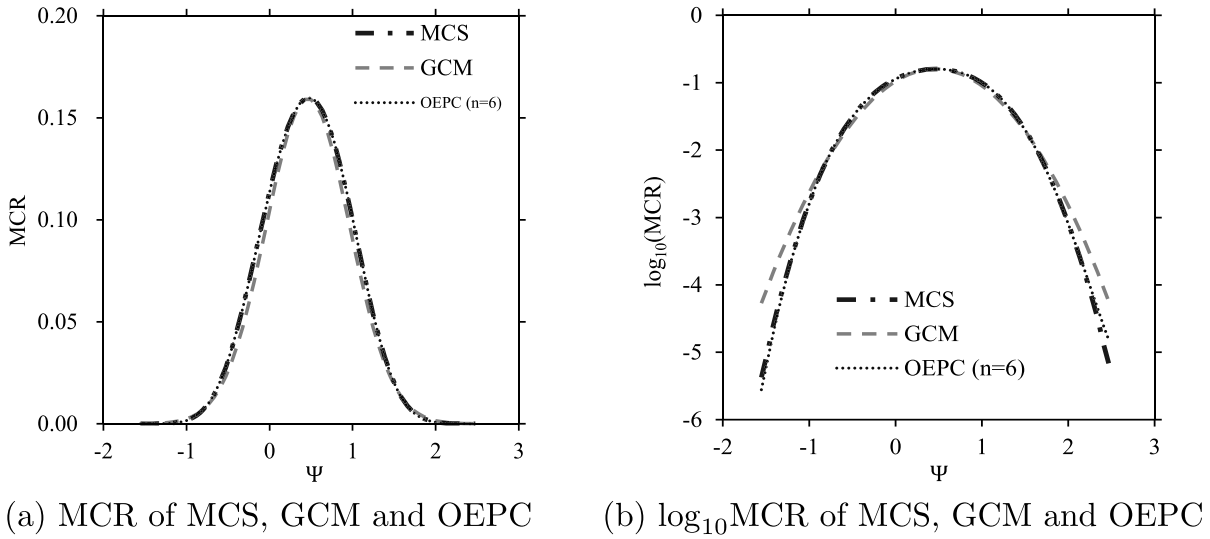

Fig. 9 MCR and Logarithmic MCR (Example 3)

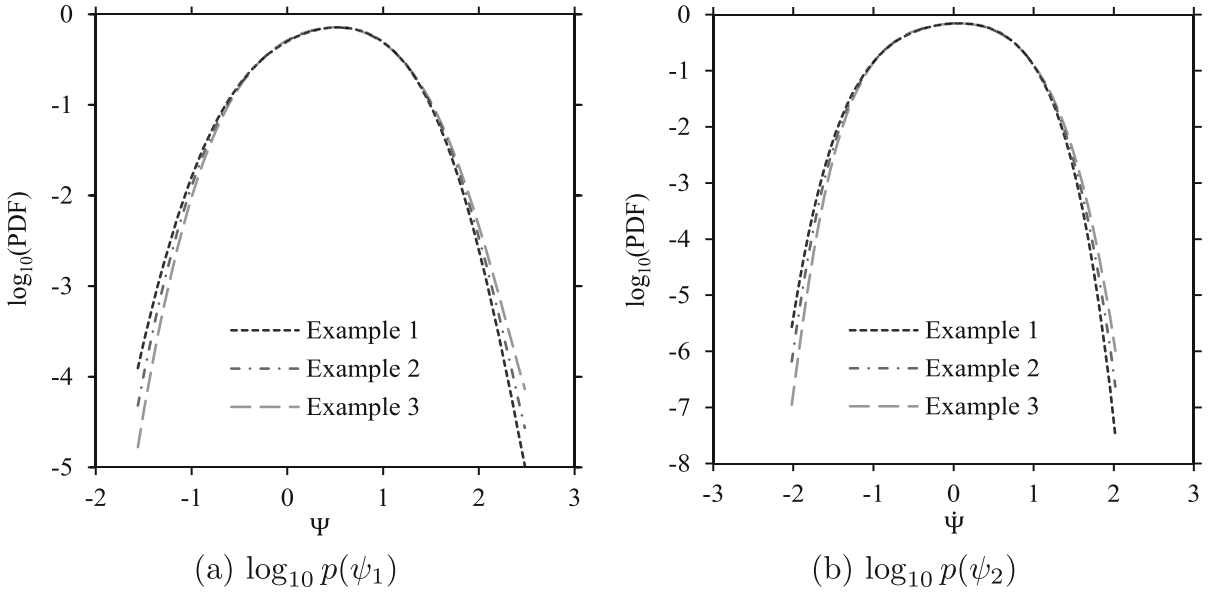

Fig. 10 Logarithmic PDF comparison (OEPC)

Figs. 4 and 1. Consequently, the density and peak position of the contour lines exhibit slight variations corresponding to the changes in correlation coefficients.

Furthermore, the comparison of Figs. 1, 4 and 7 is performed in Figs. 11, 12 and 13 within the union domain, where $\Psi \in [-1.56, 2.48]$ and $\dot{\Psi} \in [-2.02, 2.02]$.

The PDF solutions in Example 1, 2 and 3 (denoted as p_1, p_2 and p_3, respectively) are compared pairwise in Figs. 11, 12 and 13. Despite the presence of random factors in the comparison conducted by MCS, both MCS and OEPC yield similar magnitudes of solution differences. The shapes of the contour lines of OEPC and MCS are nearly identical, providing additional evidence for the credibility of this comparison. Furthermore, Figs. 11, 12 and 13 directly illustrate the influence of correlation coefficients on the system.

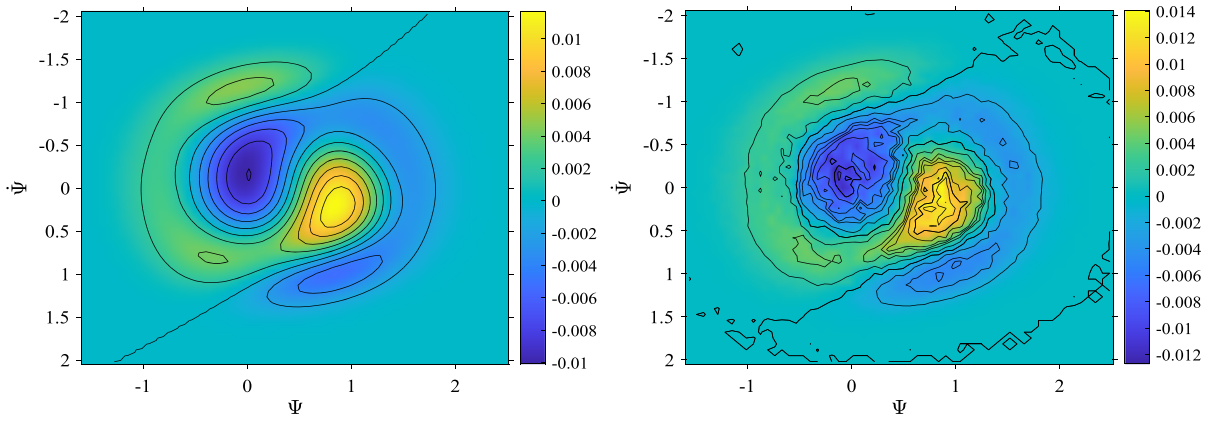

(a) $p_1 - p_2$ of OEPC (b) $p_1 - p_2$ of MCS

Fig. 11 PDF comparison between Example 1 (p_1) and Example 2 (p_2)

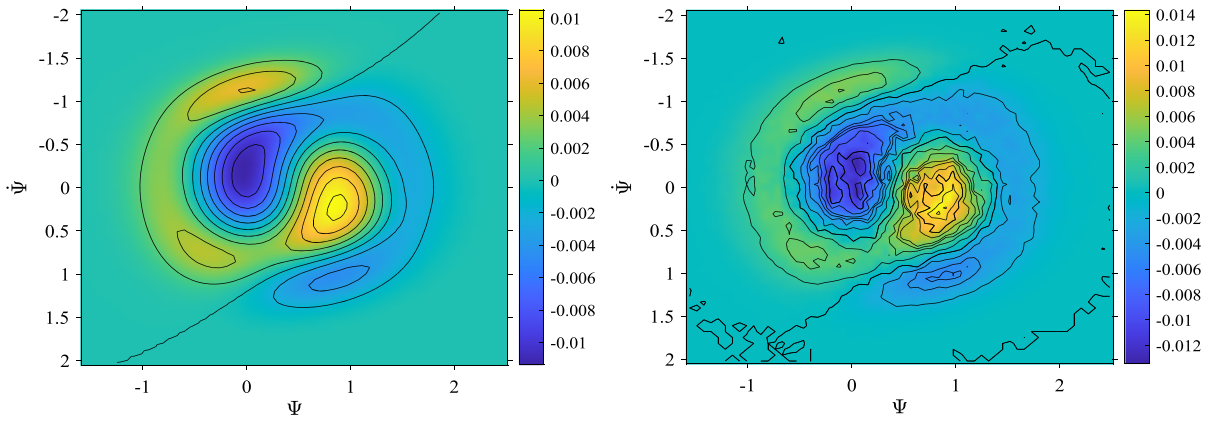

(a) $p_2 - p_3$ of OEPC (b) $p_2 - p_3$ of MCS

Fig. 12 PDF comparison between Example 2 (p_2) and Example 3 (p_3)

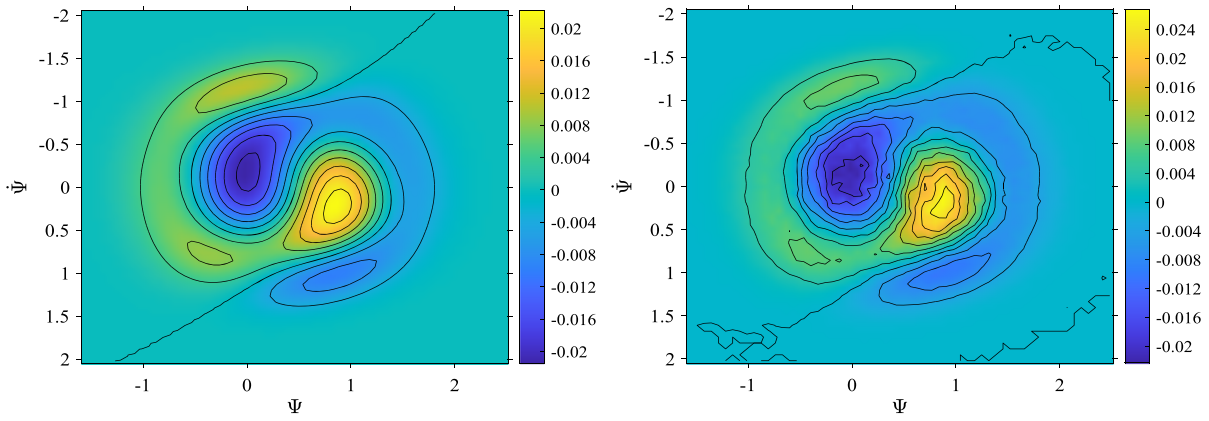

(a) $p_1 - p_3$ of OEPC (b) $p_1 - p_3$ of MCS

Fig. 13 PDF comparison between Example 1 (p_1) and Example 3 (p_3)

Table 3 Comparison of α_i values between OEPC ($n = 6$) and PEPC ($n = 6$) in Example 4

i	OEPC	PEPC	i	OEPC	PEPC
1	1.549	1.539	15	−0.09590	−0.08653
2	0.1112	0.08337	16	0.04558	0.01618
3	−1.580	−1.489	17	−0.1606	−0.1332
4	0.5575	0.5498	18	0.05200	−0.01648
5	−0.6921	−0.6881	19	−0.01433	−0.02174
6	0.7211	0.7315	20	0.06181	−0.01303
7	−0.07479	−6.691E−03	21	0.06162	0.07354
8	0.4726	0.4758	22	3.717E−03	0.01236
9	−0.2642	−0.1314	23	0.2302	0.2655
10	−0.6418	−0.7296	24	0.1061	0.1500
11	−0.1632	−0.1743	25	0.2412	0.2721
12	−1.609	−1.749	26	0.05284	0.08147
13	−1.047	−1.091	27	−0.01111	−0.03458
14	−1.402	−1.339			

Table 4 Error measurement in Example 4

Function \ Vector $\boldsymbol{\alpha}$	$\boldsymbol{\alpha}$ (OEPC)		$\boldsymbol{\alpha}$ (PEPC)
$\Theta(\boldsymbol{\alpha})$ (OEPC)	3.248E-03	$<$	6.372E-03
$\Lambda(\boldsymbol{\alpha})$ (PEPC)	2.698E-03	$>$	2.948E-07

In summary, the correlation between noise sources has an impact on the pattern of PDF solutions. In a 2D PDF image, the variation of the correlation coefficient can changes the density and peak position of the contour lines. In the logarithmic marginal PDF plot, changing the correlation coefficient induces variations in the length of curve's left and right arms, thereby influencing the tail behavior of PDF solutions.

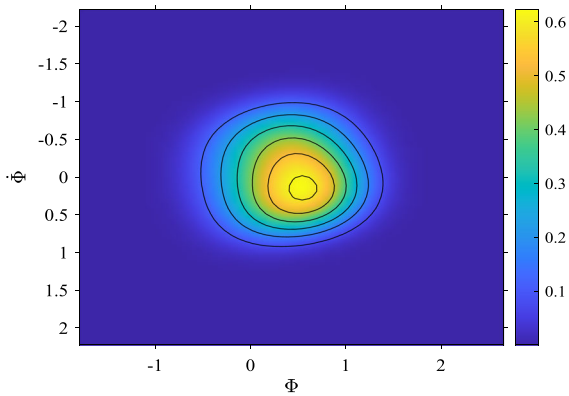

Fig. 14 $p(\psi_1, \psi_2)$ from OEPC (Example 4)

4.5 Example 4 (system of stronger nonlinearity)

In order to evaluate the accuracy of the solution for a system with higher nonlinearity, the values of c_1 and c_2 from Example 2 are doubled in this example. Consequently, c_1 is set to 0.4 and c_2 to 0.8 for the ensuing analysis. To facilitate a comparison between the results obtained from the OEPC method and the standard EPC method, Table 3 illustrates the values of $\boldsymbol{\alpha}$ ($n = 6$) from the two methods. In the subsequent discussion, the standard EPC method, which utilizes the projection solution procedure, is denoted as PEPC.

As listed in Table 3, the values of α_i obtained from OEPC and PEPC are not identical, indicating that these two methods are not equivalent.

The difference between the two methods can also be demonstrated by substituting the two different $\boldsymbol{\alpha}$ back into their respective solution procedures to measure the resulting errors. The error measurement function of OEPC is adopted as the OBJ $\Theta(\boldsymbol{\alpha})$. Meanwhile, the error from the PEPC method is measured by

$$\Lambda(\boldsymbol{\alpha}) = ||\boldsymbol{\mathcal{L}}(\boldsymbol{\alpha})|| \tag{29}$$

where Λ denotes the error measurement function of PEPC; $||*||$ refers to Euclidean norm; $\boldsymbol{\mathcal{L}}$ is a vector, and $\mathcal{L}_i$ ($i = 1, 2, \ldots, N$) denotes the algebraic equation formulated by PEPC, which can be expressed as

$$\mathcal{L}_i(\boldsymbol{\alpha}) = \int_{\mathbb{R}^2} r_n(\boldsymbol{\psi}; \boldsymbol{\alpha}) \hat{p}_2(\boldsymbol{\psi}) \psi_1^{j-k} \psi_2^k d\psi_1 d\psi_2 \tag{30}$$

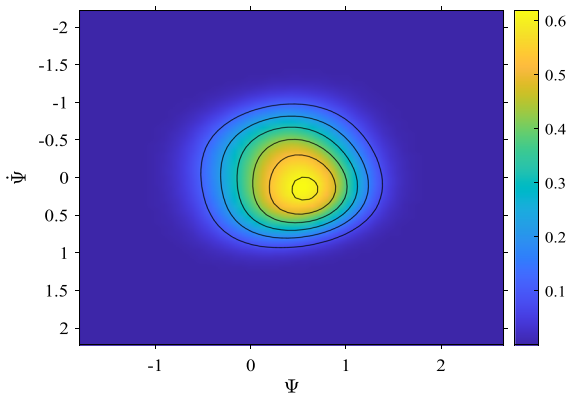

Fig. 15 $p(\psi_1, \psi_2)$ from PEPC (Example 4)

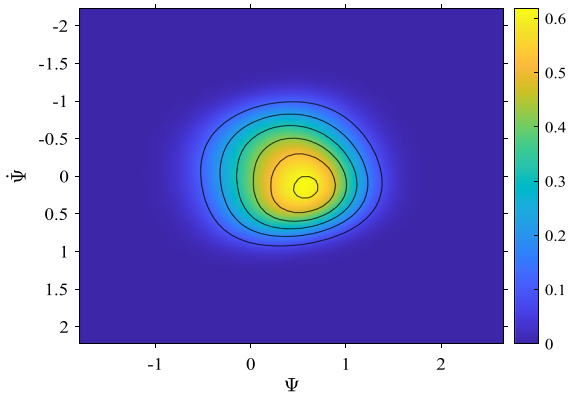

Fig. 16 $p(\psi_1, \psi_2)$ from MCS (Example 4)

where $i = \frac{j(j+1)}{2} + k$; $j = 1, 2, \ldots, n$; $k = 0, 1, \ldots, j$.

The errors are measured and listed in Table 4. It is observed that both OEPC and PEPC successfully minimize the errors in their respective solution procedures. This observation further confirms the distinction between the two methods.

In Figs. 14, 15 and 16, it can be observed that the solutions of PEPC and OEPC exhibit remarkable similarity to those of MCS, indicating the effectiveness of both methods. The bivariate PDFs are plotted within the range of $m \pm 5\sigma$, where $m_1 = 0.4297$, $m_2 = 0$, $\sigma_1 = 0.4376$ and $\sigma_2 = 0.4376$ are the values provided by GCM.

In Fig. 17, both PEPC and OEPC perform well in the range of $[m - 4\sigma, m + 4\sigma]$. However, the tail of the PEPC has lifted a bit near $m_1 + 5\sigma_1$. The trend of the curve suggests that the OEPC method has a slight advantage over the PEPC method. The sample size of MCS is increased to 10^9 in this example to show more PDF tails in $[m - 5\sigma, m + 5\sigma]$, resulting in a time consumption of 8882 s. However, even with the sample size being 10^9, the tails from MCS still can not cover the entire range of $[m_2 - 5\sigma_2, m_2 + 5\sigma_2]$. In contrast, the PEPC only takes 12 s and the OEPC takes 72 s. Therefore, both OEPC and PEPC exhibit higher efficiency compared to MCS. The total time of OEPC (72 s) is the sum of the time spent by GCM (2.33s) and the time spent on formulation and optimization procedures (69.91s).

Regarding the MCR depicted in Fig. 18a, the solutions from PEPC and OEPC align well with MCS. However, in Fig. 18b, for the lo garithmic MCR, the tail trend of OEPC demonstrates enhanced alignment with MCS. This suggests that the OEPC method effectively captures the tail behavior in PDF and MCR analysis.

5 Conclusions

The current study presents a new optimization-oriented EPC approach to solve the reduced FPK equation, aiming to explore the probabilistic solutions of the stochastic systems that incorporate both even and odd nonlinear terms in velocity, under the correlated multiplicative excitation on powered velocity and additive excitation being Gaussian white noises. In contrast to the conventional EPC solution procedure, the OEPC method introduces a substitution for the projection solution procedure by implementing an optimization-oriented procedure. This change results in the formulation of the OBJ as the integration of squared residual error. By introducing the weight function, the spatial integration in the OBJ can be calculated analytically, which simplifies the computation and improves the accuracy of the integral procedure. In addition, the initial values of the unknown parameters are also provided to ensure the convergence of the solution in optimization. To comprehensively evaluate the OEPC approach, four examples with different correlated excitations are provided. In the analysis, we investigate the joint PDFs of displacement and velocity, as well as the marginal PDF solutions and MCRs. Our findings suggest that the OEPC method not only provides improved solution accuracy compared to GCM but also demonstrates superior efficiency compared to MCS. Furthermore, the impact of correlation coefficients is discussed by collectively analyzing the first three examples. It can be concluded that the variation of correlation coefficients can impact both the contour lines and tail behavior of the PDF solutions. In

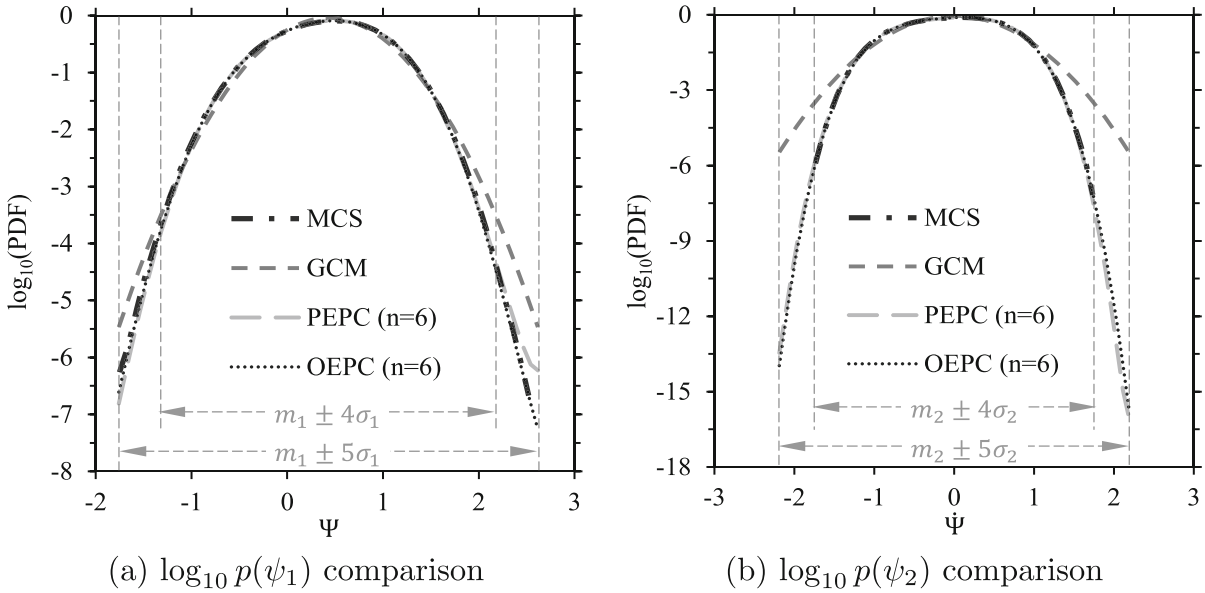

Fig. 17 Logarithmic marginal PDF solutions of the responses Ψ and $\dot{\Psi}$ and their comparison (Example 4)

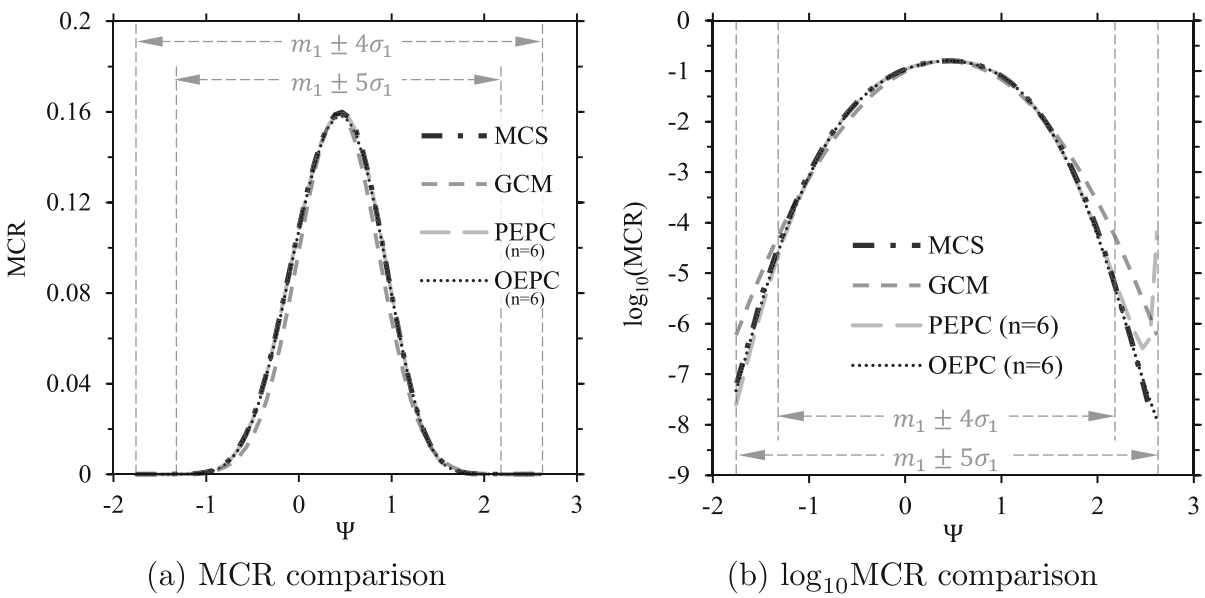

Fig. 18 MCR and Logarithmic MCR (Example 4)

Example 4, the OEPC method also exhibits improved PDF and MCR solutions in their remote tails in the case of strong system nonlinearity as compared to the traditional EPC method. Consequently, the OEPC method provides an option for analyzing stochastic nonlinear oscillators under correlated multi-power velocity multiplicative excitation and additive excitation.

Funding The results presented in this paper were obtained under the supports of the Research Committee of University of Macau (Grant No. MYGR2022-00169-FST).

Data availability The datasets analyzed in the study are available on request.

Declarations

Conflict of interest The authors declare that there is no conflict of interest.

References

1. Lin, Y.K., Cai, G.Q.: Probabilistic Structural Dynamics: Advanced Theory and Applications. McGraw-Hill, USA (1995)
2. Leira, B.J.: Optimal Stochastic Control Schemes Within a Structural Reliability Framework. Springer, London (2013)
3. Mahrenholtz, O., Bardowicks, H.: Aeroelastic problems at masts and chimneys. J. Wind Eng. Ind. Aerodyn. **4**(3–4), 261–272 (1979)
4. Mahrenholtz, D., Bardowicks, H.: Wind-induced oscillations of some steel structures. In: Practical Experiences with Flow-Induced Vibrations, IAHR/IUTAM Symposium, pp. 643–649 (1980). Springer, Berlin
5. Zhao, L., Ge, Y.: Emergency measures for vortex-induced vibration of human bridge. In: The 2020 World Congress on Advances in Civil, Environmental, and Materials Research (ACEM20), GECE, Seoul, Korea, pp. 25–28 (2020)
6. Luongo, A., Zulli, D.: Parametric, external and self-excitation of a tower under turbulent wind flow. J. Sound Vib. **330**(13), 3057–3069 (2011)
7. Zulli, D., Luongo, A.: Bifurcation and stability of a two-tower system under wind-induced parametric, external and self-excitation. J. Sound Vib. **331**(2), 365–383 (2012)
8. Belhaq, M., Kirrou, I., Mokni, L.: Periodic and quasiperiodic galloping of a wind-excited tower under external excitation. Nonlinear Dyn. **74**, 849–867 (2013)
9. Kirrou, I., Mokni, L., Belhaq, M.: On the quasiperiodic galloping of a wind-excited tower. J. Sound Vib. **332**(18), 4059–4066 (2013)
10. Er, G.-K.: An improved closure method for analysis of nonlinear stochastic systems. Nonlinear Dyn. **17**(3), 285–297 (1998)
11. Luo, J., Er, G.-K., Iu, V.P., Lam, C.C.: Transient probabilistic solution of stochastic oscillator under combined harmonic and modulated Gaussian white noise stimulations. Nonlinear Dyn. **111**(19), 17709–17723 (2023)
12. Lin, Y.K., Kozin, F., Wen, Y.K., Casciati, F., Schuëller, G.I., Der Kiureghian, A., Ditlevsen, O., Vanmarcke, E.H.: Methods of stochastic structural dynamics. Struct. Saf. **3**(3–4), 167–194 (1986)
13. Zhu, W.Q., Huang, Z.L.: Exact stationary solutions of stochastically excited and dissipated partially integrable hamiltonian systems. Int. J. Non-linear Mech. **36**(1), 39–48 (2001)
14. Harris, C.J.: Simulation of multivariable non-linear stochastic systems. Int. J. Numer. Methods Eng. **14**(1), 37–50 (1979)
15. James, F.: Monte carlo theory and practice. Rep. Prog. Phys. **43**(9), 1145 (1980)
16. Hammersley, J.: Monte Carlo Methods. Springer, Singapore (2013)
17. Xiao, M., Geng, G., Li, G., Li, H., Ma, R.: Analysis on dynamic precision reliability of high-speed precision press based on Monte Carlo method. Nonlinear Dyn. **90**, 2979–2988 (2017)
18. Natarajan, H., Popov, P., Jacobs, G.: A high-order semi-lagrangian method for the consistent Monte-Carlo solution of stochastic Lagrangian drift-diffusion models coupled with Eulerian discontinuous spectral element method. Comput. Methods Appl. Mech. Eng. **384**, 114001 (2021)
19. Booton, R.C.: Nonlinear control systems with random inputs. IRE Trans. Circuit Theory **1**(1), 9–18 (1954)
20. Takewaki, I.: Design-oriented ductility bound of a plane frame under seismic loading. J. Vib. Control **3**(4), 411–434 (1997)
21. Wang, B., Liu, J., Tang, B., Xu, M., Li, Y.: Dynamic performance of the energy harvester with a fractional-order derivative circuit. J. Vib. Control **29**(7–8), 1498–1509 (2023)
22. Iyengar, R.N., Dash, P.K.: Study of the random vibration of nonlinear systems by the Gaussian closure technique. ASME J. Appl. Mech. **45**(2), 393–399 (1978)
23. Takewaki, I.: Design-oriented ductility bound of a plane frame under seismic loading. J. Vib. Control **2**(4), 415–429 (1996)
24. Kong, F., Spanos, P.D.: Stochastic response of hysteresis system under combined periodic and stochastic excitation via the statistical linearization method. J. Appl. Mech. **88**(5), 051008 (2021)
25. Wiener, N.: The average of an analytic functional. Proc. Natl. Acad. Sci. USA **7**(9), 253–260 (1921)
26. Yu, J.S., Cai, G.Q., Lin, Y.K.: A new path integration procedure based on Gauss-Legendre scheme. Int. J. Non-linear Mech. **32**(4), 759–768 (1997)
27. Liqin, L., Yougang, T.: Stability of ships with water on deck in random beam waves. J. Vib. Control **13**(3), 269–280 (2007)
28. Di Matteo, A., Di Paola, M., Pirrotta, A.: Path integral solution for nonlinear systems under parametric Poissonian white noise input. Prob. Eng. Mech. **44**, 89–98 (2016)
29. Sun, J.-Q.: Random vibration analysis of a non-linear system with dry friction damping by the short-time Gaussian cell mapping method. J. Sound Vib. **180**(5), 785–795 (1995)
30. Zhang, Z., Dai, L.: The application of the cell mapping method in the characteristic diagnosis of nonlinear dynamical systems. Nonlinear Dyn. **111**(19), 18095–18112 (2023)
31. Sun, J.-Q., Xiong, F.-R., Schütze, O., Hernández, C.: Cell Mapping Methods: Algorithmic Approaches and Applications. Springer, Singapore (2019)
32. Mavromatis, I.G., Kougioumtzoglou, I.A., Spanos, P.D.: An extrapolation approach within the Wiener path integral technique for efficient stochastic response determination of nonlinear systems. Int. J. Non-linear Mech. **160**, 104646 (2024)
33. Zhang, Y., Kougioumtzoglou, I.A., Kong, F.: Exploiting expansion basis sparsity for efficient stochastic response determination of nonlinear systems via the Wiener path integral technique. Nonlinear Dyn. **107**(4), 3669–3682 (2022)
34. Zhu, W.Q.: Stochastic averaging methods in random vibration. ASME Appl. Mech. Rev. **41**(5), 189–199 (1988)
35. Xu, M., Jin, X., Wang, Y., Huang, Z.: Stochastic averaging for nonlinear vibration energy harvesting system. Nonlinear Dyn. **78**, 1451–1459 (2014)
36. Li, M., Liu, D., Li, J.: Stochastic analysis of vibro-impact bistable energy harvester system under colored noise. Nonlinear Dyn. **111**(18), 17007–17020 (2023)
37. Wojtkiewicz, S.F., Johnson, E.A., Bergman, L.A., Grigoriu, M., Spencer, B.F.: Response of stochastic dynamical sys-

tems driven by additive Gaussian and Poisson white noise: solution of a forward generalized Kolmogorov equation by a spectral finite difference method. Comput. Methods Appl. Mech. Eng. **168**(1), 73–89 (1999)
38. Xue, J.-R., Zhang, Y.-W., Niu, M.-Q., Chen, L.-Q.: Harvesting electricity from random vibrations via a nonlinear energy sink. J. Vib. Control 10775463221134962 (2023)
39. Hu, H., Chen, L., Qian, J.: Random vibration analysis of nonlinear structure with viscoelastic nonlinear energy sink. J. Vib. Control, 10775463231181645 (2023)
40. Cao, Q., Hu, S.-L.J., Li, H.: Nonstationary response statistics of fractional oscillators to evolutionary stochastic excitation. Commun. Nonlinear Sci. Numer. Simul. **103**, 105962 (2021)
41. Er, G.-K.: A new non-Gaussian closure method for the PDF solution of non-linear random vibrations. In: Proceedings of The ASCE 12th Engineering Mechanics Conference, pp. 1403–1406. ASCE, San Diego, USA (1998)
42. Er, G.-K., Zhu, H.T., Iu, V.P., Kou, K.P.: Probabalistic solution of nonlinear oscillators under external and parametric Poisson impulses. Am. Inst. Aeronaut. Astronaut. J. **46**(11), 2839–2847 (2008)
43. Zhu, H.: Nonzero mean response of nonlinear oscillators excited by additive Poisson impulses. Nonlinear Dyn. **69**, 2181–2191 (2012)
44. Er, G.-K., Iu, V.P.: Probabilistic solutions of a nonlinear plate excited by Gaussian white noise fully correlated in space. Int. J. Struct. Stab. Dyn. **17**(09), 1–18 (2017)
45. Er, G.-K., Iu, V.P., Du, H.-E.: Probabilistic solutions of a stretched beam discretized with finite difference scheme and excited by Kanai–Tajimi ground motion. Arch. Mech. **71**, 433–457 (2019)
46. Er, G.-.K., Iu, V.P., Wang, K., Guo, S.-S.: Stationary probabilistic solutions of the cables with small sag and modeled as mdof systems excited by gaussian white noise. Nonlinear Dyn. **85**(3), 1887–1899 (2016)
47. Chen, L., Liu, J., Sun, J.-Q.: Stationary response probability distribution of SDOF nonlinear stochastic systems. ASME J. Appl. Mech. **84**(5) (2017)
48. Sun, Y., Hong, L., Yang, Y., Sun, J.-Q.: Probabilistic response of nonsmooth nonlinear systems under Gaussian white noise excitations. Phys. A **508**, 111–117 (2018)
49. Wang, K., Zhu, Z., Xu, L.: Transient probabilistic solutions of stochastic oscillator with even nonlinearities by exponential polynomial closure method. J. Vib. Control **28**(9–10), 1086–1094 (2022)
50. Zhu, Z., Gong, W., Yu, Z., Wang, K.: Investigation on the epc method in analyzing the nonlinear oscillators under both harmonic and gaussian white noise excitations. J. Vib. Control, pp. 1–15 (2022)
51. Guo, S.-S., Meng, F.-F., Shi, Q.: The generalized EPC method for the non-stationary probabilistic response of nonlinear dynamical system. Probab. Eng. Mech. **72**, 1–15 (2023)
52. Guo, S.-S., Shi, Q., Xu, Z.-D.: Probabilistic solution for an MDOF hysteretic degrading system to modulated nonstationary excitations. Acta Mech. **234**, 1105–1120 (2023)
53. Broyden, C.G.: The convergence of a class of double-rank minimization algorithms 1. general considerations. IMA J. Appl. Math. **6**(1), 76–90 (1970)
54. Fletcher, R.: A new approach to variable metric algorithms. Comput. J. **13**(3), 317–322 (1970)
55. Goldfarb, D.: A family of variable-metric methods derived by variational means. Math. Comput. **24**(109), 23–26 (1970)
56. Shanno, D.F.: Conditioning of quasi-newton methods for function minimization. Math. Comput. **24**(111), 647–656 (1970)
57. Dennis, J.E., Jr., Moré, J.J.: Quasi-newton methods, motivation and theory. SIAM Rev. **19**(1), 46–89 (1977)
58. Berahas, A.S., Byrd, R.H., Nocedal, J.: Derivative-free optimization of noisy functions via quasi-Newton methods. SIAM J. Optim. **29**(2), 965–993 (2019)
59. Bukshtynov, V.: Computational Optimization: Success in Practice. CRC Press (2023)
60. Chapra, S.C.: Numerical Methods for Engineers. Mcgraw-hill (2010)
61. Davidon, W.C.: Variable metric method for minimization. SIAM J. Optim. **1**(1), 1–17 (1991)
62. Mishra, S.K., Ram, B.: Introduction to Unconstrained Optimization with R. Springer (2019)
63. Sreeraj, P., Kannan, T., Maji, S.: Prediction and optimization of weld bead geometry in gas metal arc welding process using RSM and fmincon. J. Mech. Eng. Res **5**(8), 154–165 (2013)
64. Ji, W., Shao, T.: Finite element model updating for improved box girder bridges with corrugated steel webs using the response surface method and fmincon algorithm. KSCE J. Civ. Eng. **25**(2), 586–602 (2021)
65. Novac, M., Vladu, E., Novac, O., Gordan, M.: Aspects regarding the optimization of the induction heating process using fmincon, minimax functions and simple genetic algorithm. J. Electr. Electron. Eng. **2**(2), 64–70 (2009)
66. Grigoriu, M.: Crossings of non-Gaussian translation processes. J. Eng. Mech. **110**(4), 610–620 (1984)
67. Naess, A., Gaidai, O.: Monte Carlo methods for estimating the extreme response of dynamical systems. J. Eng. Mech. **134**(8), 628–636 (2008)
68. Hagen, Ø., Tvedt, L.: Vector process out-crossing as parallel system sensitivity measure. J. Eng. Mech. **117**(10), 2201–2220 (1991)
69. Li, C.-Q., Firouzi, A., Yang, W.: Closed-form solution to first passage probability for nonstationary lognormal processes. J. Eng. Mech. **142**(12), 1–9 (2016)
70. Er, G.-K.: Crossing rate analysis with a non-gaussian closure method for nonlinear stochastic systems. Nonlinear Dyn. **14**, 279–291 (1997)
71. Guo, S.-S., Er, G.-K., Lam, C.C.: Probabilistic solutions of nonlinear oscillators excited by correlated external and velocity-parametric Gaussian white noises. Nonlinear Dyn. **77**, 597–604 (2014)